AIAA Aerodynamic Testing Conference March 9-10, 1964, Wash., D.C.

TWO NEW FREE-FLIGHT METHODS FOR OBTAINING CONVECTIVE-HEAT-TRANSFER DATA

By Dale L. Compton* and Gary T. Chapman*
Vehicle Environment Division
NASA, Ames Research Center, Moffett Field, Calif.

Summary

Two techniques are described for measuring convective heating to small models in free-flight ranges and tunnels.

In the first technique, called the catcher-calorimeter technique, models are gun-launched into the Ames pressurized ballistic range at velocities from 4,300 to 11,000 ft/sec, allowed to decelerate aerodynamically to a few hundred feet per second, and caught. The total aerodynamic heat input to the models is measured in a calorimeter. Extreme care is taken to account for and minimize all extraneous sources of heat addition or loss. The calorimeter was designed especially for this application and is capable of measuring heat inputs as low as 10^{-5} Btu. Measurements of convective heating to a hemisphere show good agreement with theoretical computations.

In the second technique, called the melting-onset technique, aluminum hemispheres are gun-launched into the prototype of the Ames hypersonic free-flight facility at a velocity of 24,000 ft/sec into still air, and at a combined velocity of 36,000 ft/sec into the countercurrent airstream. At some point on the flight path, the model begins to melt, and molten aluminum streams from the model surface into the wake where it can be detected in shadowgraphs. The stagnation-point heating rate is then deduced by computing the heating rate required to produce melting at the observed time. Tests conducted at 24,000 ft/sec are considered calibration tests for the technique and show its workability. Tests conducted at 36,000 ft/sec yield heating rates which are in accord with theories that predict a small effect of ionization on convective heating.

AUTHOR

Introduction

Ballistic ranges and free-flight tunnels have been little used to measure convective heating. The reason for this is that it has been difficult to determine the rate of temperature rise of the model surface. Although considerable effort has been made to develop miniature telemeter systems for this purpose, the comparatively little data obtained show the difficulty of this approach. This paper presents two different, yet complementary, approaches to the measurement of convective heating in free flight on small models.

The first method measures the total aerodynamic heat transferred to a model. This is accomplished by recovering the model at low speeds after it has been decelerated from a high initial velocity by aerodynamic drag. The heat content of the recovered model is then accurately measured in a calorimeter; a series of tests at various launch velocities is then analyzed to yield heat-transfer rates. One of the limitations of this method is that if the heating rate to the model becomes high enough - by increasing launch velocity - the model will begin to melt and lose material, and the calorimeter will fail to measure the total heat. This particular limitation of the first method becomes the basis for the second method.

The second method is based on the detection of the time of onset of melting of the model. Melting onset on free-flight aluminum models can be detected, since the molten aluminum runoff apparently forms a fine mist in the wake of the model causing a characteristic change in shadowgraphs. Surface melting on the model occurs first where the heating rate is highest - at the stagnation point. The time at which melting first occurs is a measure of the stagnation-point heating rate.

The present paper describes these two techniques in detail and presents heat-transfer data obtained. The techniques are treated separately in their historical order.

Symbols

a	thermal diffusivity of model material
b,d	groupings defined by equation (16)
A_c	maximum cross-sectional area
A_w	wetted area
c	specific heat of the model material
C_D	total drag coefficient
h	enthalpy
K	thermal conductivity of model material
K_1,K_2	constants of proportionality
m	model mass
n	exponent in equation (6)
p	pressure
Q_{aero}	total aerodynamic heat transfer
ΔQ	energy added to calorimeter
$\dot{q}$	heat-transfer rate
$\dot{q}_{av}$	heat-transfer rate defined by equation (5)
$\dot{q}_l$	local heat-transfer rate
r	reference radius
T	temperature
T_c	temperature of the calorimeter

*Research Scientist

For presentation at the AIAA Aerodynamic Testing Conf., Wash., D.C., 9-10 Mar. 1964

T_m	temperature of the model
t	time
V	velocity
x	distance along the flight path
y	distance into the model from the stagnation point, normal to the surface
β	grouping in equation (15)
γ	factor of proportionality in equation (13)
ρ	density of the air
τ	dummy variable of integration

Subscripts

catch	conditions just prior to entering catcher
i	conditions prior to launch
L	launch conditions
r	recovery conditions
st	stagnation conditions
w	wall (model surface) conditions
∞	free-stream conditions

Catcher-Calorimeter Technique

The test arrangement for the catcher-calorimeter technique is shown schematically in figure 1. A model, held in a sabot, is launched from a gun. The model, after being stripped of its sabot, enters the ballistic range and is photographed at spark shadowgraph stations while decelerating. The model scale, model material, air density, and range length are selected so that the model slows to a speed of a few hundred feet per second before entering a catcher. The model then pierces several sheets of paper, decelerates to zero-forward velocity, and falls through a paper funnel into a calorimeter where its total heat content is measured.

As the model decelerates, a major portion of its kinetic energy heats the surrounding air via the strong bow shock wave; the remaining kinetic energy is delivered to the boundary layer via skin friction and to the model surface by conduction and convection. At the beginning of the flight, the deceleration, the rate of energy loss, and the heating rate are high. As the model progresses downrange, the deceleration and the heating rate decrease. Shown in figure 2 are typical examples of a calculated heating rate history, an integrated heating history, and a calculated velocity history for the case of a 1/4-inch aluminum hemisphere at sea-level conditions. The heat-transfer rate, $\dot{q}_{av}$, shown in this figure, is the surface-averaged heat-transfer rate. All of these curves have been normalized by an appropriate maximum value. It can be seen from this figure that the major portion of the heating occurs when the velocity is still relatively high.

The experimental measurements of total heat content for various launch velocities were used to determine instantaneous heating rates.

Test Equipment and Calibration

Pressurized ballistic range and guns. Models were gun-launched into the Ames pressurized ballistic range, which is a 200-foot-long, 10-foot-diameter, pressure vessel instrumented with shadowgraph stations at various intervals. Firing times of the shadowgraph-station sparks are recorded with counter chronographs, so that the deceleration history of the model can be determined. The shadowgraph pictures also provide angle-of-attack history and flow visualization.

Both a 0.50-caliber powder-gas gun and a 0.50-caliber light-gas gun were used as model launchers - the powder-gas gun for launch velocities below 7,000 ft/sec and the light-gas gun for velocities between 7,000 and 11,000 ft/sec.

Models, sabots, and gas seals. Models used in the present tests were 1/4-inch-diameter hemispheres, machined from solid 7075 T-6 aluminum alloy. The surface finish was sufficiently smooth to maintain laminar flow at least to the model base. The diameter and material were selected to allow the model to decelerate at 1 atmosphere ambient pressure from 11,000 ft/sec to about 500 ft/sec in the 200-foot length of the range. In figure 3 a model is shown with its sabot.

The sabot, in addition to its usual functions of supporting the model during the launch and providing a seal between model and launch barrel, was designed to reduce heating to the model from three sources - barrel friction, compressed gas in front of the sabot, and driver gas behind the sabot. The protection provided by the sabot alone against the driver gas was found to be inadequate; clear evidence was obtained in early tests that propellant gas passed along the parting planes of the sabot and scorched the model. This leakage was prevented by a separate gas seal behind the sabot, the one-piece polyethylene gas seal shown in figure 3, and by several discs of 1-mil mylar placed against the base of the model.

Catcher and funnel. The catcher was designed to stop models flying at subsonic speed, intact and without appreciably altering their total heat content. The catcher consisted of 45-50 sheets of building paper (Federal specification UU-P-271-Type C), hung on a rack. Sheets were spaced about 3/4 inch apart so the model could fall freely between any two sheets into the funnel.

The funnel was formed of heavy brown wrapping paper with steep sides and squared corners. This design reduced the tendency of the model to spiral down the funnel; any such resultant delay in transit would permit additional heat loss from the model to the funnel and the air. The heat loss during transit through the catcher and funnel was small but measureable. A discussion of this loss is given in a later section of this paper.

Calorimeter. The calorimeter was designed specifically for this application. It consisted of a thin silver cup into which the model was dropped, a heat sink to absorb the heat, and a controlled conduction path between the cup and heat sink. Each of these elements had a particular function and in some cases more than one function. Figure 4 is a quarter-sectional view of the calorimeter.

The silver cup acted as a receiver for the hot model. Since the electrical signal representing model total heat was obtained from a thermopile attached to the cup, it was important to keep the heat capacity of the cup very low and the diffusivity high. Thus the silver cup had to be as small and as thin (approximately 0.003-inch wall thickness) as possible so it could come to an equilibrium temperature with the hot model rapidly and also have a fairly high temperature rise with a small heat input. The cup was instrumented with a thermopile consisting of seven iron-constantan thermocouples on the bottom exterior. Six of these were connected in series with six reference junctions located in the heat sink. The seventh thermocouple was used to determine absolute temperatures.

The heat sink was constructed of two large blocks of phosphor bronze. The silver cup was suspended in a cavity in the lower block. Buried in the lower portion of the lower block were seven iron-constantan thermocouples which utilized the heat sink as a constant temperature reference mass; six of these were the reference junctions for the cup thermopile, and the seventh was used to record absolute temperatures. The purpose of two large blocks was to provide a sufficiently large heat capacity that their temperature level would not change more than a few thousandths of a degree during a shot and while temperatures were being recorded. The upper block also served to cover the cavity where the silver cup was suspended. The model entered the cup through a conical hole in the upper block. This hole was lined with a low conductivity plastic to minimize any heat transfer due to contact with the model as it dropped through to the cup.

The principal conduction path between the cup and heat sink consisted of three small thin support arms made of low conductivity epoxy resin. These were fastened between the upper lip of the cup and the rim of the cavity. The cross section of these supports was made so that the major portion of the heat from the hot model would be transferred to the heat sink in about 10 to 15 minutes. It was necessary to use very fine thermocouples (0.001-inch-diameter wire) on the cup to minimize both their heat capacity and their conductivity between the cup and the heat sink. The excess volume of the cavity was filled with foamed plastic so that there would be no free convective heat transfer from the cup.

With the calorimeter constructed as described above, the heat transfer from the cup to heat sink can be expressed schematically as shown in sketch (a).

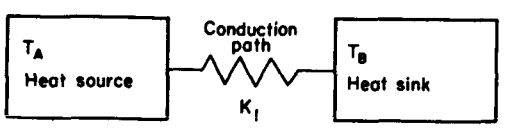

Sketch (a)

The differential equation for the conductive heat transfer from a source to a sink is

$$\frac{dQ}{dt} = K_1[T_A(t) - T_B] \tag{1}$$

thus

$$Q \equiv \Delta Q = K_1 \int_0^\infty \left[T_A(t) - T_B\right] dt \tag{2}$$

A finite integration limit of 10 to 15 minutes was used to replace the infinite limit on the integral in equation (2). This finite truncation was found to have negligible effect on the results. This was demonstrated by plotting the value of the integral with various upper limits and observing its asymptotic nature.

The output of the thermopile is proportional to the instantaneous temperature difference $T_A - T_B$. This output, in millivolts, is recorded on a strip chart recorder from which a typical trace is shown in figure 5. The output was also electromechanically integrated to obtain the area under the temperature difference time curve. Measurements of heat inputs as low as 10^{-5} Btu were found to be possible with this equipment. The development of this highly sensitive and accurate calorimeter made this test technique possible since, as will be noted in later sections, heat quantities measured in the tests were in the range from 10^{-3} to 10^{-2} Btu.

Calibration of the calorimeter. To calibrate the calorimeter preheated models were dropped into it to determine the constant K_1 in equation (1) and to determine the effects of several variables on K_1.

The calibration setup consisted of an oven suspended over the calorimeter. The model was placed in the oven, allowed to come to some known temperature, and dropped into the calorimeter. (There was a radiation shield between the oven and calorimeter at all times except during model release.) The integrated output, $\Delta Q/K_1$, of the thermopile was then read and plotted versus the calculated energy increment introduced by the hot model. This process was repeated at various model energies. The plot of calculated heat input versus integrated values of $\Delta Q/K_1$ resulted in a straight line, the slope of which was the value of K_1. The calibrations were repeated with variations of model geometry, model orientation in cup, model material, and nonuniform temperatures in the model. The model geometries for these calibrations were a 1/4-inch-diameter hemisphere, a 30° half-angle cone slightly blunted with 0.20-inch base diameter, and a 1/4-inch sphere. Most of the models were aluminum; however, other materials were used and gave essentially the same results. The condition of a nonuniform temperature distribution in the model was simulated by dropping two models at the same time but with different temperatures. The value of K_1 was found to be constant within ±3 percent.

Data Reduction

Reduction of total heat-transfer data. The reduction of the total heat-transfer data proceeds from an energy balance. The thermal energy, ΔQ,

added to the calorimeter by the model is obtained directly from the area under the ΔT versus time curve of the calorimeter and the calibration constant K_1. This increment of energy consists of two parts, the energy due to aerodynamic heating, Q_{aero}, and the energy due to possible differences in the energy levels of the model and the calorimeter prior to launching of the model. The increment in energy, ΔQ, can be expressed as

$$\Delta Q = Q_{aero} + mc(T_{m_i} - T_{c_i}) \tag{3}$$

where m is the mass of the model, c is the specific heat of the model material, and T_{m_i} and T_{c_i} are the prelaunch model and calorimeter temperatures, respectively. In equation (3) it is assumed that there are no extraneous heat sources. This was found to be a good assumption if proper precautions were taken. (See Error Analysis section for the details of these precautions.) Solving equation (3) for Q_{aero} yields

$$Q_{aero} = \Delta Q - mc(T_{m_i} - T_{c_i}) \tag{4}$$

The last term on the right, which represents the correction for differences in temperature of the model and calorimeter, was generally less than 10 percent of Q_{aero}. The temperature of the model was taken as the prelaunch gun temperature. This was insured by loading the model into the gun at least one hour before launch.

Conversion of total heat-transfer measurements to instantaneous heating rates. The total heat, Q_{aero}, measured for different launch velocities, may be further analyzed to obtain the instantaneous average heat-transfer rate over the surface as a function of velocity. The instantaneous average heating rate, $\dot{q}_{av}$, will be defined as

$$\dot{q}_{av} = \frac{1}{A_w}\int_{A_w} \dot{q}_l dA_w \tag{5}$$

where $\dot{q}_l$ is the local heat-transfer rate, and A_w is the wetted area of the body. The functional relationship between $\dot{q}_{av}$, free-stream density, and velocity is assumed to be similar to the one discussed in reference 1. This relationship is

$$\dot{q}_{av} = K_2 \sqrt{\frac{\rho_\infty}{r}}\, V_\infty^{\,n} \tag{6}$$

where ρ_∞ is the free-stream density, r is a reference length (e.g., radius of curvature at the stagnation point), V_∞ is the flight speed, and K_2 and n are constants to be determined.

The total aerodynamic heat transfer to a model during a given trajectory can be expressed as

$$Q_{aero} = A_w \int_0^t \dot{q}_{av} d\tau \tag{7}$$

where t is the time of flight.

From the equation of motion, we obtain

$$dt = \left(\frac{-2m}{C_D A_c}\right)\frac{dV}{\rho_\infty V_\infty^2} \tag{8}$$

Equations (6), (7), and (8) may be combined as

$$Q_{aero} = \frac{-K_2 2mA_w}{\sqrt{\rho_\infty r}\, A_c}\int_{V_L}^{V_{catch}} \frac{V_\infty^{\,n-2}}{C_D}\, dV \tag{9}$$

Since the velocity history and drag coefficient are known, evaluation of Q_{aero} depends only on selection of n and K_2 to give a functional dependence of Q_{aero} on launch velocity which matches that recorded experimentally from test shots at different launch velocities. The procedure for selecting n and K_2 to obtain a best fit to the experimental data is given in appendix A.

The analysis described above applies only if both K_2 and n are constant or nearly constant over the trajectory. This is true if the wall temperature is small compared to the recovery temperature, a condition which is satisfied for the part of the flight during which the major portion of heating occurred. In addition, the pitching amplitude must be small enough so that the heating is not affected. A slightly more elaborate analysis (not presented here) allows some consideration of angle-of-attack effects.

Launch velocity. The launch velocity (i.e., velocity at the muzzle of the gun) and drag coefficients were deduced from the measured distance-time history by the method of reference 2.

Typical Results

Some typical total heat-transfer data obtained with the calorimeter technique are shown in figure 6(a). These results are for a 1/4-inch-diameter aluminum hemisphere tested at 1 atmosphere free-stream pressure. These data were then analyzed, by the simple data-reduction method described earlier, to obtain instantaneous heat-transfer rates averaged over the wetted surface area. These results are shown in figure 6(b). For comparison, theoretical calculations at Mach numbers 4 and 6 by the method of Stine and Wanlass (ref. 3) are presented (squares). Further theoretical calculations were made for higher speeds using the stagnation-point results of Fay and Riddell (ref. 4) and the distributions from the method of reference 3. Calculation for several points allowed a curve to be drawn through the speed range shown. (All theoretical calculations shown are for the case of zero base heat transfer.) It can be seen that the agreement with theory is very good. The differences are no greater than 19 percent, and, in the case of the Fay and Riddell stagnation-point plus Stine and Wanlass distribution, adding a small amount to the calculated values to account for base heating would improve the agreement. Also shown is the stagnation-point heat-transfer rate calculated by the method of reference 4 upon which the second theoretical estimates were based. A more complete discussion of these data and a presentation of data from a blunted-cone model may be found in reference 5.

Error Analysis

The accuracy of the total heat-transfer measurements depends primarily upon the accuracy of the calorimeter system and the size of extraneous heat sources and sinks. The calorimeter has a maximum error of ±3 percent of the total heat transfer measured (determined from calibration). Several extraneous sources of heating were considered. These include:

1. Heating from shock-heated gases in front of the model while the model is traversing the launch tube.

2. Heating caused by propellant gas leaking through the sabot to the model.

3. Heat loss due to long subsonic flight.

4. Heating and/or cooling during capture in the catcher and funnel.

Items 1 and 2 were discussed briefly in the discussion of sabots and gas seals; however, a more detailed description of the extent to which these sources of heat were eliminated is included here. The complete enclosure of the model within the sabot, and the partial evacuation of the launch tube, are believed to completely eliminate heating resulting from item 1.

The heating resulting from item 2 was as high as 100 percent of Q_{aero} when no gas seal was used. The effectiveness of the gas seal in reducing this heating was ascertained from several test shots with gas seals of various designs. Several shots with various length gas seals were fired at the same launch velocity; when heat input was plotted versus increasing gas seal length, the curve appeared to approach an asymptote which was considered to represent zero heating by gun gases. The gas seal finally used appeared to reduce this heating to about 7 or 8 percent of Q_{aero}. (Launching problems prevented the use of a longer gas seal.) Additional heat protection, consisting of thin sheets of mylar placed over the base of the models, appeared to further reduce this heating to about 2 percent of Q_{aero}.

Heat is lost from the model during the portion of the flight when the wall temperature is greater than the recovery temperature, approximately 0.1 second. The electrical heat flow analog computer at Ames (ref. 6) was programmed to represent the thermal properties of the hemisphere model and the heat transfer to the model. The model was then "flown" from 10,000 to 1,000 ft/sec and then the front face inputs were switched to represent cooling to the atmosphere (i.e., $h_r = h_\infty$). In 0.1 second of "flight" 2 percent of the model's total heat was lost. Since the average cooling rate during subsonic flight is numerically less than the 1,000 ft/sec cooling rate employed, it can be concluded that heat losses during subsonic flight are negligible. At subsonic flight times longer than 0.2 second the cooling would increase rapidly; therefore the catch should be made at as high a subsonic speed as possible. In the present tests, catches were made between 500 and 800 ft/sec, resulting in subsonic flight times from 0.1 to 0.06 second.

Three sources of heating or cooling of the model in passing through the catcher and funnel combination were considered: deformation of the model; friction between model and paper; and conduction between model, paper, and air. The models were examined under a microscope after they had penetrated the sheets of paper and no sign of deformation was evident. It was therefore felt that the heating due to deformation was negligible. The other two sources of heat transfer were difficult to analyze, and since the models enter the catcher with kinetic energy of the same order of magnitude as the total aerodynamic heating, this extraneous heating could be large if a substantial fraction of this energy were converted to heat in the model.

To assess the amount of extraneous heating in the catcher-funnel, the heat transfer from the model to the catcher and funnel was studied experimentally. A compressed air gun was built so that the major portion of the barrel passed through a temperature-controlled oven. This gun was set up to fire into the catcher-funnel-calorimeter combination. Two series of tests were conducted with a 1/4-inch aluminum sphere as the test model. In one, the model was launched cold (i.e., at the same temperature as the catcher) to minimize conduction effects in the catcher. Launches were made at various subsonic velocities and therefore various numbers of sheets of catcher paper were penetrated. The measured heat input increased slightly with the number of sheets penetrated; it was, however, less than one-thirtieth of the kinetic energy on entry into the catcher. The second test was conducted with the model heated to between 35° and 40° F above the temperature of the catcher. In this case the difference in thermal energy (i.e., measured in the calorimeter minus calculated for the known model temperature rise) at first was negative and then increased with increasing number of sheets penetrated (increasing velocity); the net error was zero after about 28 sheets were penetrated. This indicates that, at first, the energy interchange between model and catcher is controlled by conduction losses until finally frictional heating predominates and the heating increases. The maximum errors resulting from these effects in the actual heating experiments occurred at the lower speeds where they were as high as ±10 percent of the total aerodynamic heating.

Two comments are in order as to the catcher-funnel errors. First, the paper used in this catcher was the only material tried. It is not very likely that it is the optimum from a heat-transfer standpoint. Secondly, the simple experiment indicated that even the 10-percent error could be partially eliminated if, with a setup similar to the one described, the heating in the catcher were determined carefully for each configuration to be tested. This was not done for the data presented in figure 6.

The sum of the estimated errors in the total heat measurements is listed below for three different velocities.

	Error range, percent	Launch velocity
Total aerodynamic heating, Q_{aero}	+13 -15	5,000
	+8 -10	7,000
	+6 -8	10,000

The estimated accuracy of measured drag coefficient and launch velocity is 1 percent.

Because of the method of data reduction used, it is difficult to estimate the accuracy of the heating rates, $\dot{q}_{av}$. The maximum expected error could be larger than the maximum error in the total heat-transfer measurements. As can be seen from figure 6, the difference between the heating rates obtained from the present technique and from well-established theory, for the case of a hemisphere, which is for all practical purposes a proof configuration, is near the maximum error in the total heating measurements.

Remarks

The preceding sections present a discussion of the catcher-calorimeter technique for obtaining experimental heat-transfer data at high speeds. The technique, once developed, is very simple to use. Furthermore, it has the potential of being relatively accurate compared to other heat-transfer measurement techniques. The heat-transfer results for a hemisphere were compared with theory and were found to agree very well. A disadvantage of the technique is that, in some cases, many data points are required to obtain the desired results.

Possible applications of the technique, not considered in this paper, are determination of heat transfer in gases other than air and measurement of heat absorbed by ablating bodies.

When total heating is measured with this technique, a definite high velocity limitation occurs for any model. If the velocity exceeds this limit, the model will eventually begin to ablate, and heat will be lost with the ablated material. Furthermore, the injection of ablation products into the boundary layer affects the heating rate. This limitation to the catcher-calorimeter technique becomes the basis for the melting-onset technique.

Melting-Onset Technique

This technique uses the time of onset of melting on small aluminum models as a measure of the stagnation-point heating rate. A sabot-held aluminum hemisphere is gun-launched at high velocity either into still air or into an oncoming airstream. Heating is experienced by the model as it decelerates. This heating serves to raise the temperature of the model and, if heating is prolonged, at some point along its flight path the surface of the model will begin to melt. Melting occurs first in the stagnation region, where the heating rate is highest. Since the viscosity of molten aluminum is low, aluminum flows off the model surface and into the wake. This liquid aluminum runoff produces a partially opaque screen which is visible in the wake region on spark shadowgraphs. If the free-stream density and model size are adjusted correctly, melting can be made to begin during the portion of the model flight through the instrumented test section of the range; thus the time at which melting first occurs can be determined from successive shadowgraphs. With the time of melting-onset known, the stagnation-point heating rate can be determined by solving the heat-conduction equation for the model interior. This technique is described in detail in the following sections.

Test Equipment

Models were launched from a light-gas gun into the prototype of the Ames hypersonic free-flight facility, which may be operated either as a ballistic range or as a free-flight wind tunnel. A schematic view of the facility is shown in figure 7. The model launcher used for these tests was a caliber 0.50 deformable-piston, light-gas gun. Models fly through an instrumented test section equipped with 11 spark shadowgraph stations spaced at 4-foot intervals along its length. An enlarged view of part of the test section is shown in the inset of figure 7. The shadowgraph and chronograph equipment is similar to that in the pressurized ballistic range described earlier. The time-distance history and angle-of-attack history of the model are extracted from the shadowgraph pictures and chronograph records.

When this facility is used as a free-flight wind tunnel, the airstream is supplied from a 40-foot-long, 6-1/4-inch-diameter shock tube coupled to a combustion chamber of like dimensions. The energy for driving the shock tube is supplied by the constant volume-combustion of H_2 and O_2 diluted with He and N_2. The shock-tube diaphragm is punctured when the combustion process has reached peak temperature and pressure. The initial pressure ratio is adjusted to tailor the reflected shock at the interface, producing a stagnation region of high-pressure, high-temperature air. A second diaphragm separates the stagnation region of the shock tube from the test section. This diaphragm breaks spontaneously soon after the incident shock impinges upon it, allowing flow to begin in the wind tunnel. The pressure in the test section is set prior to the run at such a level that wind tunnel starting transients are minimized. The contoured nozzle provides a nominal $M = 7$ airstream. The airstream exhausts into a large vacuum tank at the end of the test section. A more complete description may be found in reference 7.

Models and Test Conditions

The test models for this investigation were 1/4-inch-diameter 7075 T-6 aluminum hemispheres identical to those used in the catcher-calorimeter tests. The stagnation-point heating rate on this model is relatively insensitive to small angle of attack. Sabots were similar to those described in the first section of this paper but were made significantly lighter in order to obtain high launch velocities. This sabot had the same advantage for heat-transfer measurements as mentioned earlier - minimum extraneous heating during launch from the gun.

The results of two sets of tests utilizing the melting-onset technique are described in this paper. Each of these sets will be described in detail in later sections. The nominal test conditions are summarized in the following table.

Test velocity, ft/sec	24,000	36,000
Model velocity, ft/sec	24,000	24,000
Airstream velocity, ft/sec	0	12,000
ρ_∞, slugs/ft^3	1.6×10^{-4} - 2.9×10^{-4}	1.5×10^{-5}
p_∞, atm	0.066 - 0.12	.02
M_∞	21	20
T_∞, $^\circ$R	540	1700
Reynolds number based on model diameter and free-stream properties	2.1×10^5 - 3.8×10^5	1.2×10^4

Wind-Tunnel Data Reduction

To obtain heating-rate data, it is necessary to know the free-stream properties as a function of time along the flight trajectory. For the tests at 24,000 ft/sec, in which the models were fired into still air, the free-stream properties were determined from the measured temperature and pressure of the air in the tunnel immediately prior to the firing of each shot. For these tests the model, though decelerating, was flying through a constant density environment.

For the tests at 36,000 ft/sec, in which the models were fired into the supersonic airstream, a more complex situation existed. To reach the steady airstream the model must fly across the vacuum tank (see fig. 7) where properties will be very poorly defined after the entry of free-stream air. To avoid this difficulty, models were fired at such a time as to meet the airstream before it had begun to enter the vacuum tank. This procedure is illustrated in figure 8. It can be seen from this figure that the model must fly through three distinct regions: (1) the low pressure (approximately 300 microns Hg) still air in the vacuum tank and in the entrance to the test section, (2) the wind-tunnel starting shock wave and the air initially in the tunnel which has been compressed by this starting shock wave, and (3) the desired test environment - the steady hypersonic airstream. The properties in each of these regions must be determined in order to assess the contribution of each to the total heating. In region 1 the air velocity is zero, and the temperature and pressure were measured prior to each test. Both the extent of and properties in region 2 were determined from calibration tests by measuring the tunnel pitot pressure and wall static pressure as functions of time. It was determined that the model flies through region 2 for a distance of about 8 feet. The measured speed of the starting shock wave and the measured properties in region 1 were used to calculate air velocity and density immediately behind the starting shock. The density and velocity were assumed to vary linearly between their values immediately behind the starting shock and their values in region 3. The effect of these assumptions on the test results will be considered in the section on errors. The properties in region 3 were determined from measurements of (a) the pressure and temperature of the air in the shock tube prior to the run, (b) the velocity of the initial shock wave in the shock tube, and (c) the pressure behind the reflected shock wave (the stagnation pressure driving the wind tunnel). From these measurements, the stagnation enthalpy for the wind-tunnel reservoir was calculated by applying the appropriate shock-tube equations. Wind-tunnel free-stream properties (the properties in region 3) were then determined from the static pressure measured at several points on the test section wall. The real-gas flow between the reservoir and the test section was assumed to be isentropic and in equilibrium. A probe mounted in the tunnel during calibration tests showed pitot pressures consistent with predictions based on the above measurements.

Solutions to the Heat-Conduction Equation

In order to relate the melting-onset time to the heat-transfer rate, it was necessary to solve the heat-conduction equation for the interior of the model. Calculations showed that for the short flight times being considered (approximately 2 milliseconds) the appreciably heated layer within the model was thin (less than 10 percent of the model diameter), and that the one-dimensional form of the heat-conduction equation could be used. The boundary conditions are those for a semi-infinite slab, initially at uniform temperature, heated on its exposed surface with a time-dependent heating rate. The time dependence of the heating rate arises because of the changing free-stream conditions and velocity along the flight path.

Thus the equations to be solved are

$$\left.\begin{aligned} a\frac{\partial^2 T}{\partial y^2} &= \frac{\partial T}{\partial t} \qquad y > 0,\ t > 0 \\ T(y, 0) &= T_i \\ -K\left(\frac{dT}{dy}\right)_{y=0} &= \dot{q}_{st} = f(t) \end{aligned}\right\} \quad (10)$$

The solution of this system is well known and can be written with the aid of Duhamel's integral (see, e.g., ref. 8, p. 76). The surface temperature is given by

$$(T_w - T_i) = \left(\frac{a}{\pi}\right)^{1/2} \frac{1}{K} \int_0^t \dot{q}(t - \tau)\, \frac{d\tau}{\tau^{1/2}} \quad (11)$$

where $\dot{q}$ is the heating rate and the other quantities are defined in the table of symbols. Thus if the heating rate is known as a function of time, the surface-temperature variation with time may be calculated. Under the assumption of constant free-stream density (i.e., when the model is flown into still air) and constant drag coefficient, one form of the trajectory equation is

$$V = \frac{1}{\frac{\rho_\infty C_D A_c}{2m} t + \frac{1}{V_L}} \quad (12)$$

Since the velocity does not change greatly over the trajectory, the stagnation-point heating rate may

be approximated by a less general form of equation (6)

$$\dot{q}_{st} = \gamma V^3 \tag{13}$$

where γ depends on ρ_∞ and the body size.

If equations (11), (12), and (13) are combined, the equation for surface temperature may be written

$$T_w - T_i = \frac{\dot{q}_{st_L}}{KV_L^3}\sqrt{\frac{a}{\pi}}\int_0^t \frac{d\tau}{\left[\frac{\rho_\infty C_D A_c}{2m}(t-\tau) + \frac{1}{V_L}\right]^3 \tau^{1/2}} \tag{14}$$

where $\dot{q}_{st_L}$ is the heating rate at the beginning of flight. This may be integrated to give

$$T_w - T_i = \frac{2\dot{q}_{st_L}}{K}\sqrt{\frac{at}{\pi}}\left\{\frac{d^3}{8(bt+d)^2}\left[\frac{2(bt+d)+3d}{d^2} + \frac{3}{2\sqrt{bt(bt+d)}}\ln\frac{\sqrt{bt+d}+\sqrt{bt}}{\sqrt{bt+d}-\sqrt{bt}}\right]\right\}$$

$$= \frac{2\dot{q}_{st_L}}{K}\sqrt{\frac{at}{\pi}}\,\beta \tag{15}$$

where

$$b = \frac{\rho_\infty C_D A}{2m}, \quad d = \frac{1}{V_L} \tag{16}$$

and β is the term in braces. Equation (15) is a closed-form solution for the time dependence of the stagnation-point surface temperature for models fired into still air.

When the models are fired through the tunnel starting transient flow into the countercurrent airstream, it is no longer possible to obtain a closed form solution and equation (11) must be integrated numerically. The integral is improper at its lower limit and thus unsuitable for numerical integration. A slight alteration to equation (11) removes the singularity to give

$$(T_w - T_i) = 2\sqrt{\frac{a}{\pi}}\frac{1}{K}\int_0^{\sqrt{t}} \dot{q}_{st}(t-\tau)\, d(\sqrt{\tau}) \tag{17}$$

The numerical integration of equation (17) was programmed for the IBM 7090 computer. Equation (17) will allow the surface temperature to be computed as a function of time for countercurrent airstream operation if the heating rates along the flight path are known.

Calibration Tests at 24,000 ft/sec

To check the validity of the melting-onset technique, several tests were performed at conditions for which the heating rate is well known from the work of previous experimenters (ref. 9). As shown in the tabulated test conditions, the velocity chosen for these tests was nominally 24,000 ft/sec and free-stream densities were varied from 1.6×10^{-4} to 2.9×10^{-4} slugs/ft^3. These tests were performed without the countercurrent airstream. The procedure was to examine critically all the shadowgraphs from a run to determine at which station melting was first observed. The inputs to equation (15) were then determined, with the initial heating rate computed from the theory of reference 4, and the stagnation-point surface temperature was computed as a function of time. A typical set of data from one of these runs is shown in figure 9. This figure shows successive shadowgraphs from the first six wind-tunnel stations. Nothing unusual is seen in the flow field behind the model until station 3, where slight wisps of aluminum appear at the rear corners of the model. This shows that melting started before the model reached station 3 and probably after it passed station 2. As the model progresses downrange through the shadowgraph stations, more and more aluminum is visible at the shoulders and in the wake. Finally, the model is distorted by the loss of material. Shown on this figure are the elapsed times of flight to each station and the model surface temperatures at each station computed from equation (15). It is significant that melting is first observed at almost exactly the time when the computed surface temperature reaches the melting temperature of 7075 T-6 aluminum (1180° F). This provides a check on the validity of the technique and leads to confidence in its use at velocities where the heating rate is not well known.

The results of all the tests at 24,000 ft/sec are presented in figure 10. This figure is a correlation plot of the predicted value of $\beta\sqrt{t}$ from equation (15) for T_w = 1180° F versus the measured value for melting onset. This coordinate system allows errors to appear linearly on the plot. The 45° line is the line of perfect correlation and it can be seen that the data lie extremely close to this line. It was not always possible to be as certain of the station in which melting first began as in the run shown on figure 9. Thus the data are presented as bars in figure 10, which indicate the $\beta\sqrt{t}$ range from the time at which melting was first probable until it was first surely in evidence. These data scatter around the 45° line by +9 percent to -13 percent. Thus within these limits the data are repeatable.

Tests at 36,000 ft/sec

Since the calibration tests showed the technique to be usable, tests were conducted at a velocity of 36,000 ft/sec. At this velocity, as well as at higher velocities, the effect of ionized species on convective heat transfer has been in question and data gathered by an independent measuring technique are of considerable value.

The tests at 36,000 ft/sec were conducted in a countercurrent airstream which had a nominal velocity of 12,000 ft/sec. The melting-onset time was determined in the same manner as in the lower speed tests. The calculation of heating rate from

the melting-onset time is complicated as noted earlier by the variety of free-stream conditions which the model encounters. The technique of data reduction was to assume heating-rate histories along the trajectory, consistent with the variations of velocity and density encountered, and to compute the time-temperature history at the stagnation point from equation (17). The time at which the stagnation point was calculated to reach 1180° F was then compared with the time at which melting was first observed. The heating-rate equation was adjusted accordingly until a history was found for which the two times matched. Since, as will be shown in the next section, the major portion of the heating occurred in region 3 (see fig. 8), the calculation of the surface temperature is relatively insensitive to the choice of heating rates in regions 1 and 2.

The data obtained in the 36,000 ft/sec tests are shown in figure 11. They fall with the majority of the shock-tube data (refs. 10, 11, and 12) and support theories which predict that the effect of ionized species on convective heat transfer in air will be small (refs. 11, 13, 14, 15, and 16). They lie approximately a factor of 2 below the theory of reference 17. There are, however, some shock-tube data which are substantially above the present data and the majority of the shock-tube data (refs. 18 and 19). Gruszczynski (ref. 19) has reported that this difference can be traced to the type of heat-transfer gage used; the higher data were obtained with nickel and nickel alloy gages and the lower data with platinum gages. This difference has not yet been explained. The present method uses a different material - 7075 T-6 aluminum - and the method itself is sufficiently different from the shock-tube methods to be considered independent. These facts lend considerable support to the lower data. However, until a satisfactory explanation is found for the higher data, all results should be viewed cautiously.

Error Considerations

As with all heat-transfer techniques, sources of error in the present technique are difficult to evaluate completely. If the calibration tests are considered alone, the deviation of the heating rate from the average is +9 and -13 percent. Part of this can be accounted for by the fact that the model is observed only at discrete times along the flight path, and therefore, melting onset is always observed sometime after it might first have been observed. On the average this error is ±6 percent. Therefore, other sources of error, for example, changes in heating during launch, changes in sabot separation from run to run, and angle of attack, must account for the remainder of the deviation in the calibration tests.

For the tests conducted at 36,000 ft/sec additional sources of error are due to the uncertain free-stream properties. The properties in region 2 (see fig. 8) are the least well determined and it is desirable to estimate the effect of this uncertainty on the heating. A breakdown of the calculated heating distribution along the flight path is given in the following table:

Region	Percent of heating
1	6
2	19
3	75

It can be inferred from this table that even relatively large errors in determining the properties in region 2 will not produce large errors in the deduced heat-transfer rates for region 3, since region 2 contributes a relatively small percentage of the total heating.

The sum of errors due to imperfect knowledge of the airstream is impossible to assess accurately, but it is believed that they will be of the order of 5 to 10 percent. Thus the over-all accuracy of these tests is estimated to be 16 to 21 percent. It should be noted that the internal consistency of the data points at 36,000 ft/sec is of this order.

Remarks

This technique, which measures local heating rates, is relatively simple to use. It has potential for use at very high velocities - in excess of earth escape velocity. Testing times are of the order of 10 to 100 times longer than in shock tubes. There are, however, sources of error, particularly when the countercurrent airstream is used, which are difficult to assess. In general, the accuracy of the technique can be considered acceptable but not extraordinary. Its principal virtue is that it is different from other techniques and thus offers an independent method for obtaining experimental data.

Possible applications of the technique not considered in the present paper are the measurement of heat transfer in planetary gases, the study of the effects of surface catalycity on heat transfer, and the measurement of heat-transfer rates to other parts of the model.

Conclusions

This paper has discussed two techniques to measure convective heat transfer in free-flight facilities. The major conclusions are:

1. Both techniques are sufficiently different from other methods for measuring convective heat transfer to be considered independent.

2. Both methods are simple to use, requiring little additional equipment over that normally found in free-flight ranges and tunnels.

3. The methods are reasonably accurate - less than ±15 percent uncertainty for the catcher-calorimeter method and about ±20 percent for the melting-onset method.

4. Both methods have been used to obtain data. The velocity range covered is from 4,300 to 36,000 ft/sec, in which the data show good agreement with theories and with other existing data.

5. The data at 36,000 ft/sec (a) support theories which show small effects of ionized species on convective heating, and (b) agree with the majority of existing shock-tube data.

Appendix

Reduction Of The Total Heat-Transfer Data To Heat-Transfer Rates

The total heat absorbed by a nonablating vehicle in decelerating flight is given by equation (9) of the text as

$$Q_{aero} = \frac{-K_2 2mA_w}{\sqrt{\rho_\infty r}\, A_c} \int_{V_L}^{V_{catch}} \frac{V^{n-2}}{C_D}\, dV \qquad (A1)$$

For the case of constant drag coefficient, equation (A1) can be integrated directly to give

$$Q_{aero} = \frac{K_2 2mA_w}{\sqrt{\rho_\infty r}\, A_c C_D (n-1)} \left(V_L^{n-1} - V_{catch}^{n-1} \right) \qquad (A2)$$

In all cases the launch velocity is much greater than the catch velocity and the value of n, as determined by theory and substantiated experimentally, is usually about 3; therefore,

$$V_L^{n-1} \gg V_{catch}^{n-1}$$

and equation (A2) reduces to

$$Q_{aero} = \frac{K_2 2mA_w}{\sqrt{\rho_\infty r}\, A_c C_D (n-1)} V_L^{n-1} \qquad (A3)$$

If equation (A3) is physically realistic, we see that the total aerodynamic heating should be a power-law function of the launch velocity; therefore a plot of Q_{aero} versus launch velocity on a logarithmic plot results in a straight line, the slope of which is equal to the exponent $(n-1)$, and the constant K_2 is the value of Q_{aero} at the 1-foot-per-second intercept. Figure 6(a) shows that the data obtained do fall in an approximately straight line. A systematic method of applying equation (A1) which allows variation in C_D and is a least squares fit to the available data was therefore developed as follows.

Least Squares Analysis

In the least squares analysis the model velocity was assumed to be known exactly. The sum of the residuals σ can be written as

$$\sigma = \sum \left(Q_{aero_{exp}} - \frac{K_2 2mA_w}{\sqrt{\rho_\infty r}\, A_c} \int_{V_L}^{V_{catch}} \frac{V^{n-2}}{C_D}\, dV \right)^2 \qquad (A4)$$

where the subscript exp refers to the experiment, and the summation extends over all the experimental points. The derivative of equation (A4) with respect to K_2 set equal to zero yields the value of K_2 for a particular n which minimizes the sum of the residuals for that value of n:

$$\frac{d(\sigma)}{dK_2} = 2 \sum \left(Q_{aero_{exp}} - BK_2 \int_{V_L}^{V_{catch}} \frac{V^{n-2}}{C_D}\, dV \right) B$$

$$\int_{V_L}^{V_{catch}} \frac{V^{n-2}}{C_D}\, dV = 0 \qquad (A5)$$

where

$$B = \frac{2m}{\sqrt{\rho_\infty r}} \frac{A_w}{A_c}$$

Thus, the best fitting value of K_2 is given by

$$K_2 = \frac{\sum Q_{aero_{exp}} B \int_{V_L}^{V_{catch}} \frac{V^{n-2}}{C_D}\, dV}{\sum \left(B \int_{V_L}^{V_{catch}} \frac{V^{n-2}}{C_D}\, dV \right)^2} \qquad (A6)$$

This procedure was applied for several trial values of n and the corresponding sums of the residuals were plotted versus n. The value of n at the minimum of this curve along with the corresponding value of K_2 was selected as the best fit to the data. This graphical selection is equivalent to taking the derivative of equation (A4) with respect to n setting it equal to zero and solving that equation and (A5) simultaneously for K_2 and n; the graphical method, however, is simpler.

References

1. Chapman, Dean R.: An Approximate Analytical Method for Studying Entry Into Planetary Atmospheres. NACA TN 4276, 1958.

2. Seiff, Alvin: A New Method for Computing Drag Coefficients From Ballistic Range Data. Jour. Aero. Sci., vol. 25, no. 2, Feb. 1958, pp. 133-134.

3. Stine, Howard A., and Wanlass, Kent: Theoretical and Experimental Investigation of Aerodynamic-Heating and Isothermal Heat-Transfer Parameters on a Hemispherical Nose With Laminar Boundary Layer at Supersonic Mach Numbers. NACA TN 3344, 1954.

4. Fay, J. A., and Riddell, F. R.: Theory of Stagnation Point Heat Transfer in Dissociated Air. Jour. Aero. Sci., vol. 25, no. 2, Feb. 1958, pp. 73-85, 121.

5. Chapman, Gary T., and Jackson, Charles T., Jr.: Measurement of the Heat Transfer to Bodies of Revolution in Free Flight by Use of a Catcher Calorimeter. NASA TN D-1890, 1963.

6. Neel, Carr B.: Cooling of Structures in High Speed Flight. North Atlantic Treaty Organization Advisory Group for Aeronautical Research and Development. AGARD Rep. 210, Oct. 1958.

7. Seiff, Alvin: A Progress Report on the Ames Hypervelocity Free-Flight Facilities and Some of the Current Research Problems Being Studied in Them. Presented at AIAA National Summer Meeting, Los Angeles, June 17-20, 1963.

8. Carslaw, H. S., and Jaeger, J. C.: Conduction of Heat in Solids. Second ed. Oxford Univ. Press, London, 1959.

9. Rose, P. H., and Stark, W. I.: Stagnation Point Heat-Transfer Measurements in Dissociated Air. Jour. Aero. Sci., vol. 25, no. 2, Feb. 1958, pp. 86-97.

10. Rose, P. H., and Stankevics, J. O.: Stagnation Point Heat Transfer Measurements in Partially Ionized Air. Res. Rep. 143, Avco-Everett Res. Lab., April 1963.

11. Hoshizaki, H.: Heat Transfer in Planetary Atmospheres at Super-Satellite Speeds. ARS Jour., vol. 32, no. 10, Oct. 1962, pp. 1544-51.

12. Offenhartz, E., Weisblatt, H., and Flagg, R. F.: Stagnation Point Heat Transfer Measurements at Super-Satellite Speeds. Jour. of the Royal Aero. Soc., vol. 66, no. 613, Jan. 1962, p. 54.

13. Howe, J. T., and Viegas, J. R.: Solutions of the Ionized Radiating Shock Layer Including Reabsorption and Foreign Species Effects and Stagnation Region Heat Transfer. NASA TR R-159, 1963.

14. Cohen, Nathaniel B.: Boundary-Layer Similar Solutions and Correlation Equations for Laminar Heat-Transfer Distribution in Equilibrium Air at Velocities up to 41,000 Feet Per Second. NASA TR R-118, 1961.

15. Adams, Mac C.: A Look at the Heat Transfer Problem at Super-Satellite Speeds. ARS paper no. 1556-60, American Rocket Society, New York, Dec. 1960.

16. Pallone, A., and Van Tassell, W.: Stagnation Point Heat Transfer for Air in the Ionization Regime. ARS Jour., vol. 32, no. 3, March 1962, pp. 436-7.

17. Scala, Sinclaire M., and Warren, Walter R.: Hypervelocity Stagnation Point Heat Transfer. ARS Jour., vol. 32, Jan. 1962.

18. Warren, W. R., Rogers, D. A., and Harris, C. J.: The Development of an Electrically Heated, Shock Driven Test Facility. Second Symposium on Hypervelocity Techniques, Denver, 1962.

19. Gruszczynski, J. S., and Warren, W. R., Jr.: Experimental Heat Transfer Studies of Hypervelocity Flight in Planetary Atmospheres. Gen. Elec. Co. Presented at Conference on Physics of Entry into Planetary Atmospheres, M.I.T., Aug. 26-28, 1963. AIAA paper no. 63-450.

FIGURE LEGENDS

Figure 1.- Schematic drawing of test setup.

Figure 2.- Typical variations in heating and velocity with distance from the gun.

Figure 3.- Sectional drawing of a typical model, sabot, and gas seal.

Figure 4.- Quarter-sectional drawing of the calorimeter.

Figure 5.- Typical calorimeter output trace.

Figure 6.- Heat transfer to a 0.25-inch-diameter hemisphere at 1 atmosphere free-stream pressure. (a) Total aerodynamic heat transfer. (b) Comparison of the experimental and theoretical heat-transfer rates, based on front face wetted area, for a 0.25-inch-diameter hemisphere.

Figure 7.- Schematic drawing of prototype hypersonic free-flight facility.

Figure 8.- Schematic for air-on operation. Not to scale.

Figure 9.- Shadowgraphs showing onset of melting.

Figure 10.- Correlation plot for 24,000 ft/sec data.

Figure 11.- Data taken at 36,000 ft/sec.

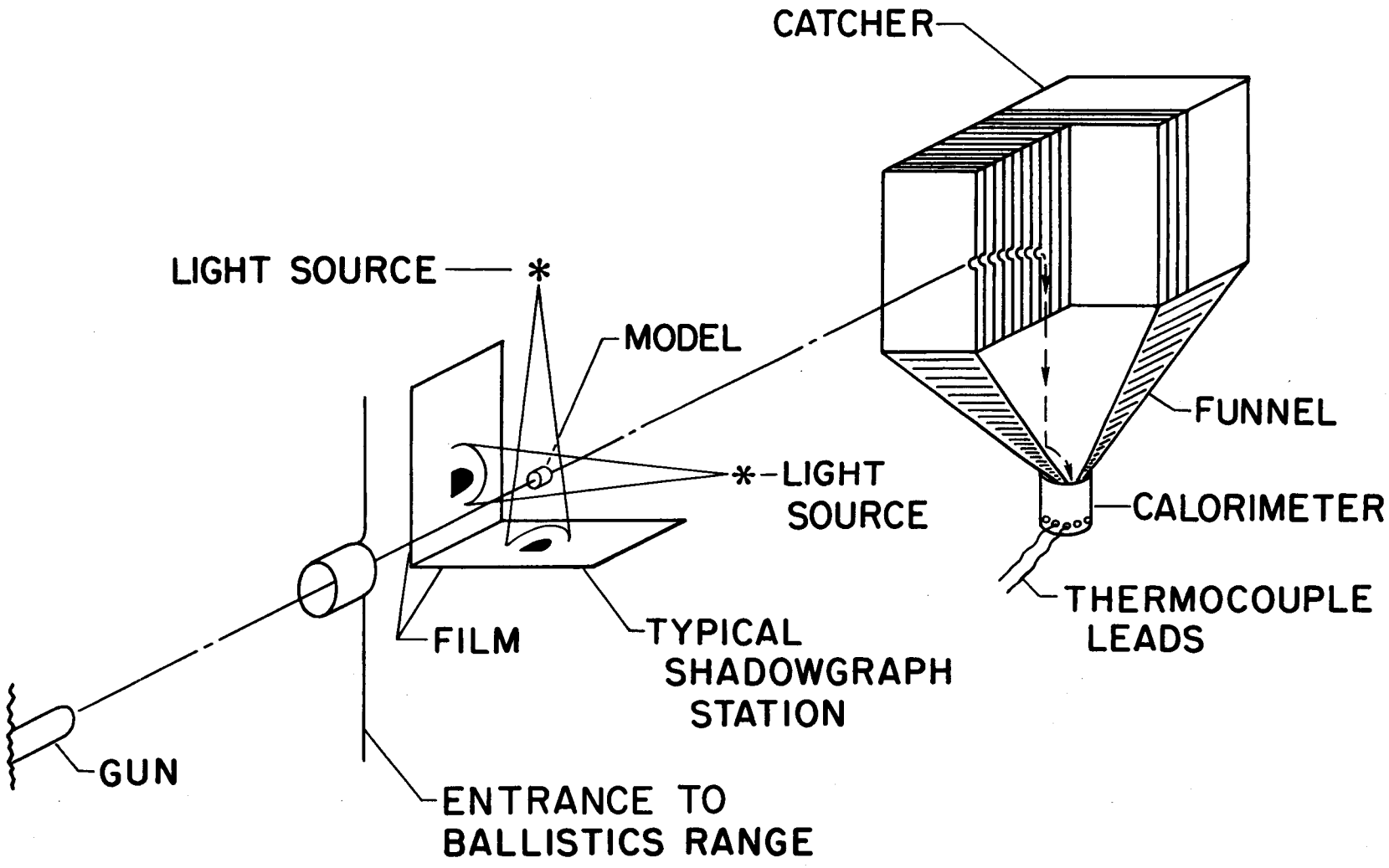

Figure 1.- Schematic drawing of test setup.

NATIONAL AERONAUTICS AND SPACE ADMINISTRATION
AMES RESEARCH CENTER, MOFFETT FIELD, CALIFORNIA

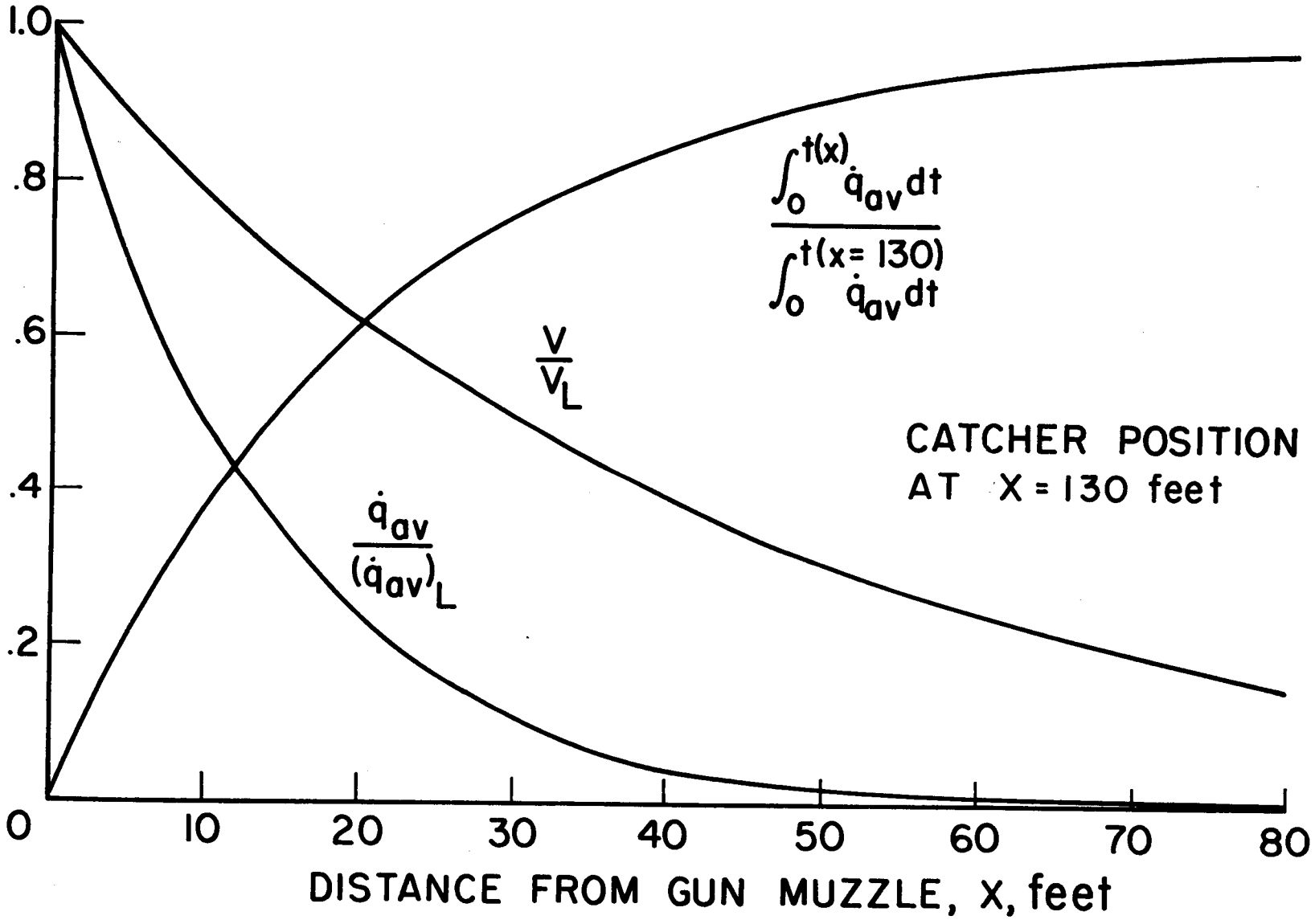

Figure 2.- Typical variations in heating and velocity with distance from the gun.

NATIONAL AERONAUTICS AND SPACE ADMINISTRATION
AMES RESEARCH CENTER, MOFFETT FIELD, CALIFORNIA

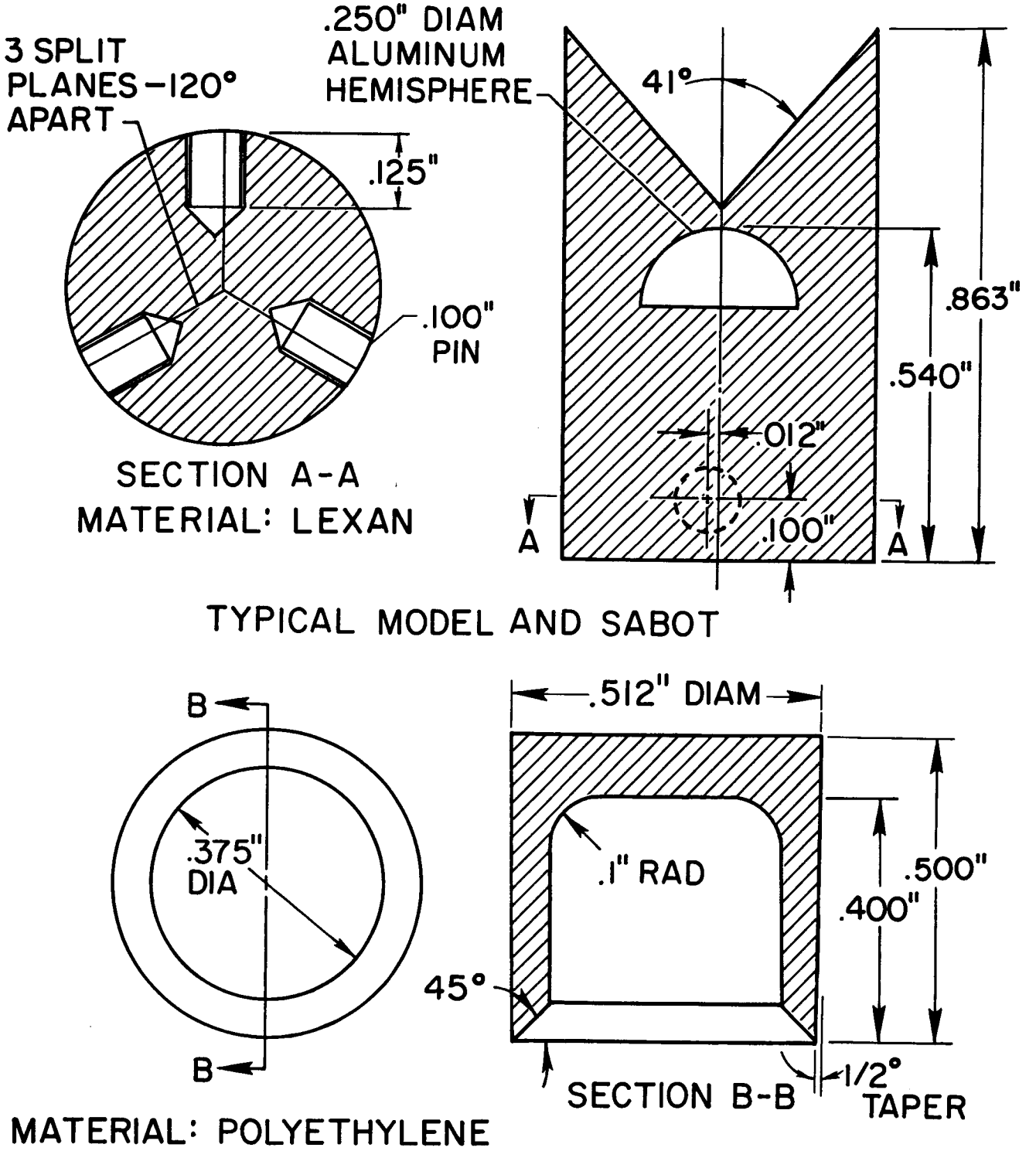

Figure 3.- Sectional drawing of typical model, sabot, and gas seal.

NATIONAL AERONAUTICS AND SPACE ADMINISTRATION
AMES RESEARCH CENTER, MOFFETT FIELD, CALIFORNIA

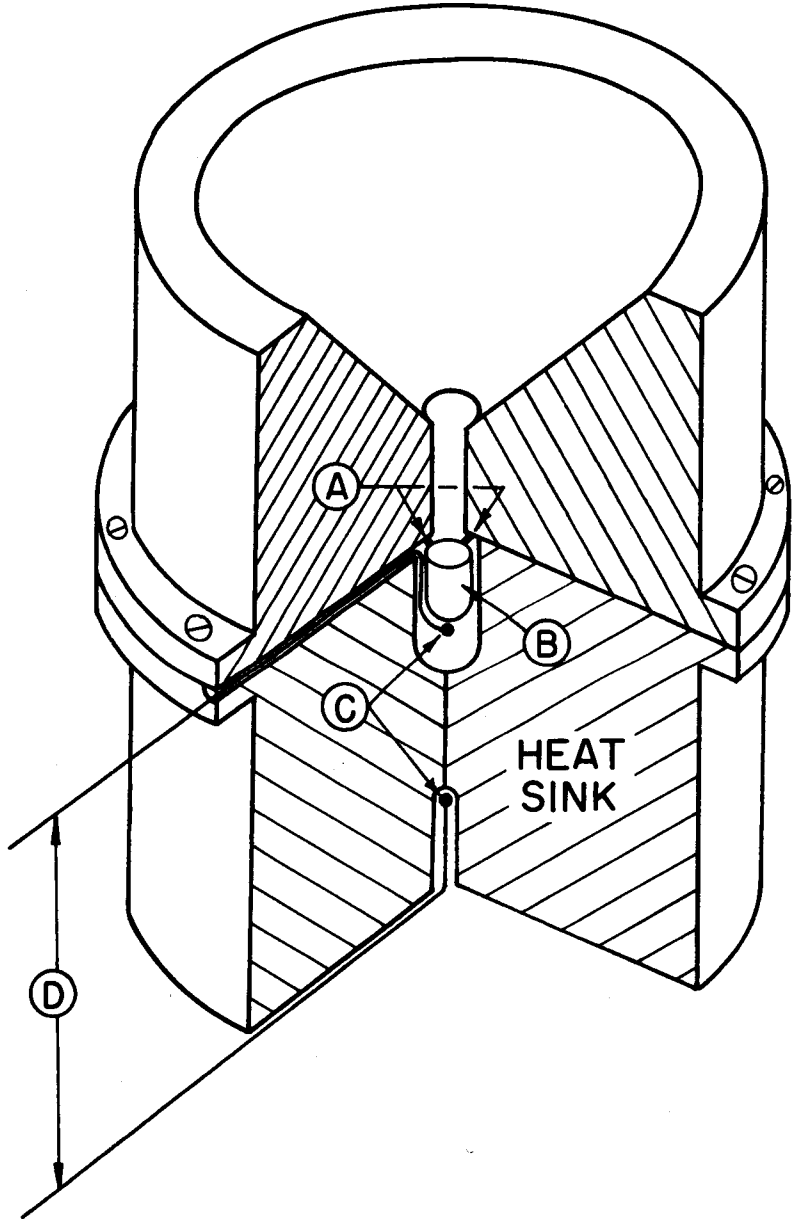

Ⓐ CUP SUPPORTS (CONDUCTION PATH)

Ⓑ SILVER CUP ~ 2.0×10^{-3} lb

Ⓒ THERMOCOUPLES

Ⓓ THERMOCOUPLE LEADS

Figure 4.- Quarter-sectional drawing of the calorimeter.

NATIONAL AERONAUTICS AND SPACE ADMINISTRATION
AMES RESEARCH CENTER, MOFFETT FIELD, CALIFORNIA

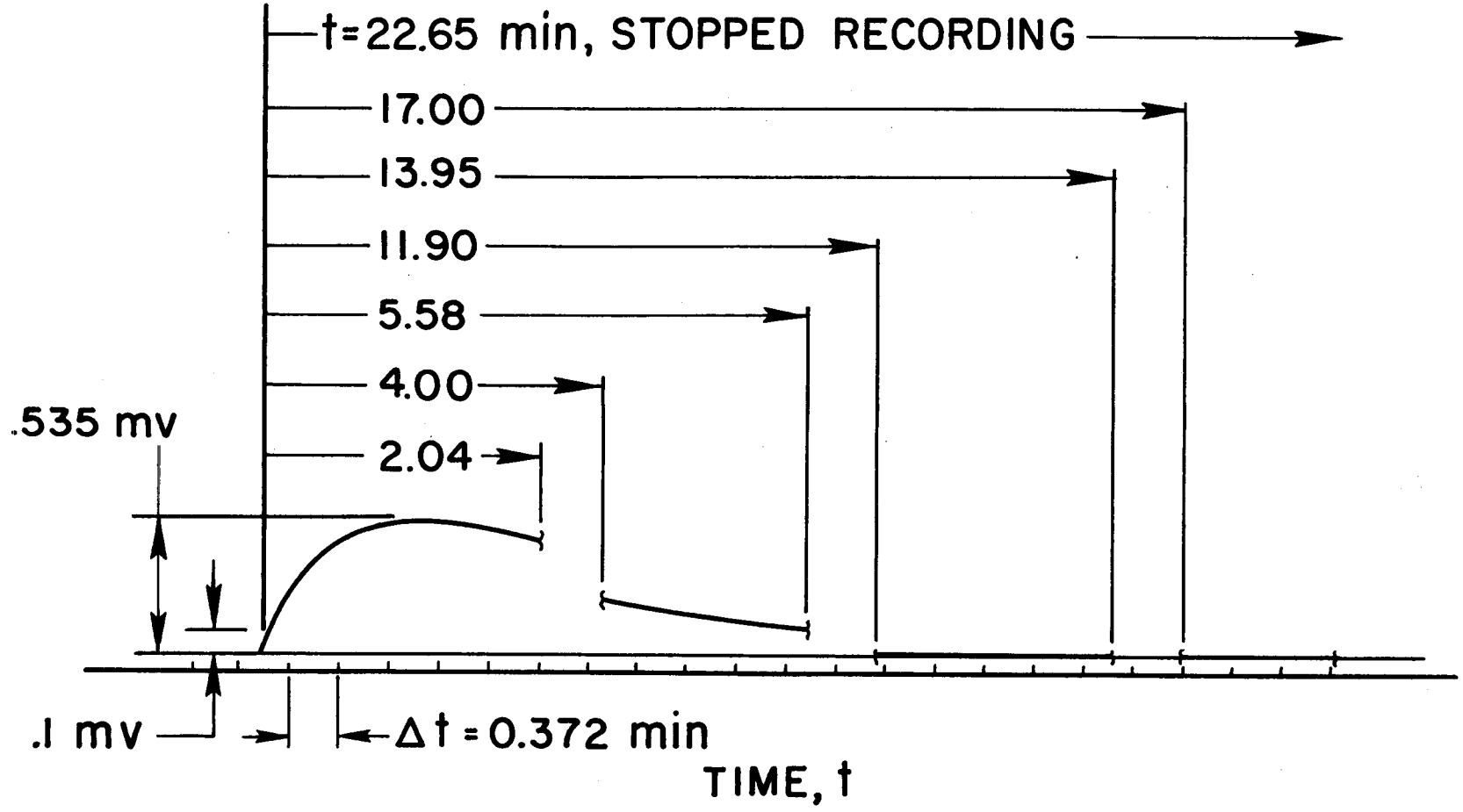

Figure 5.- Typical calorimeter output trace.

NATIONAL AERONAUTICS AND SPACE ADMINISTRATION
AMES RESEARCH CENTER, MOFFETT FIELD, CALIFORNIA

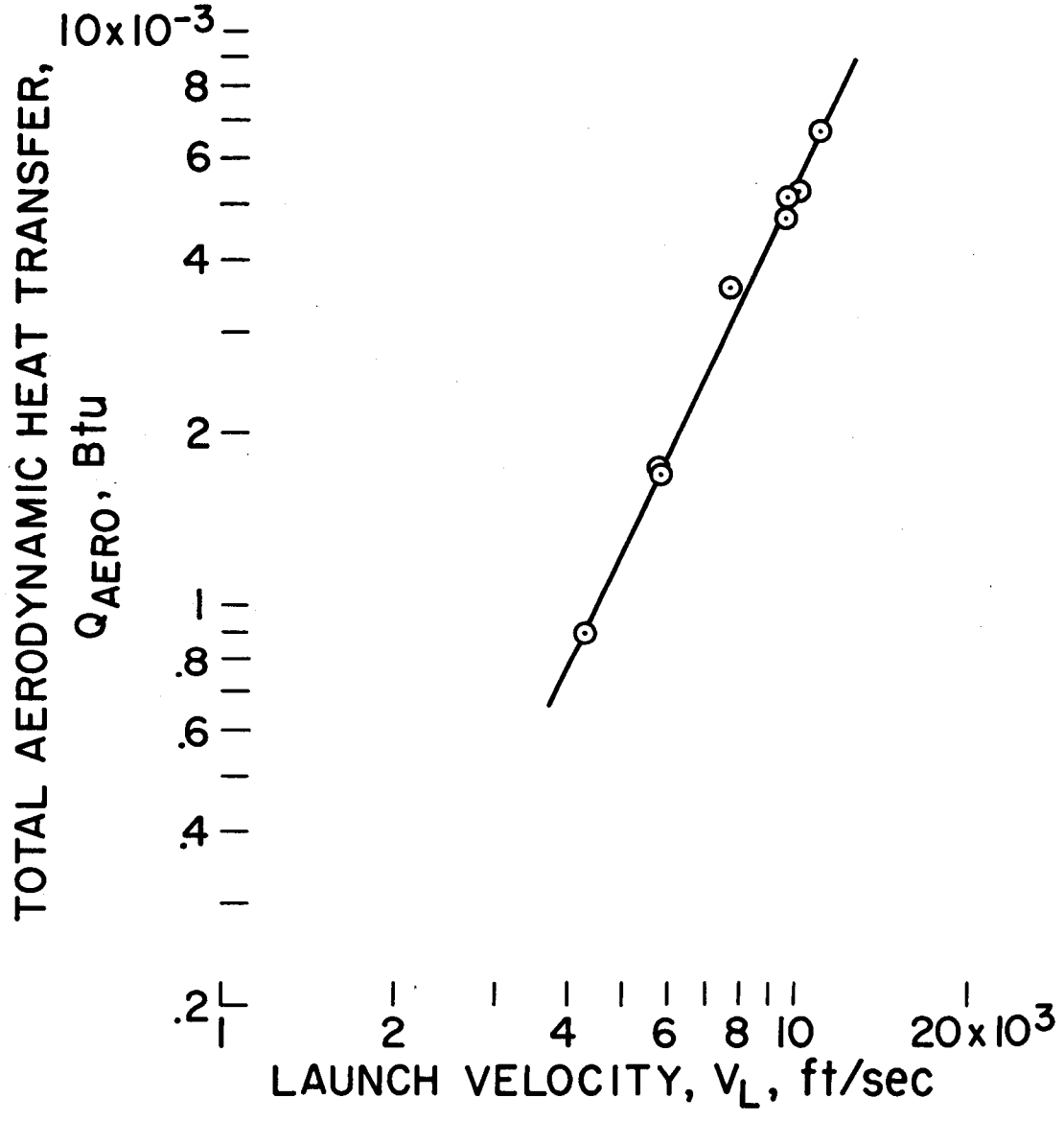

(a) Total aerodynamic heat transfer.

Figure 6.- Heat transfer to a 0.25-inch-diameter hemisphere at 1 atmosphere free-stream pressure.

NATIONAL AERONAUTICS AND SPACE ADMINISTRATION
AMES RESEARCH CENTER, MOFFETT FIELD, CALIFORNIA

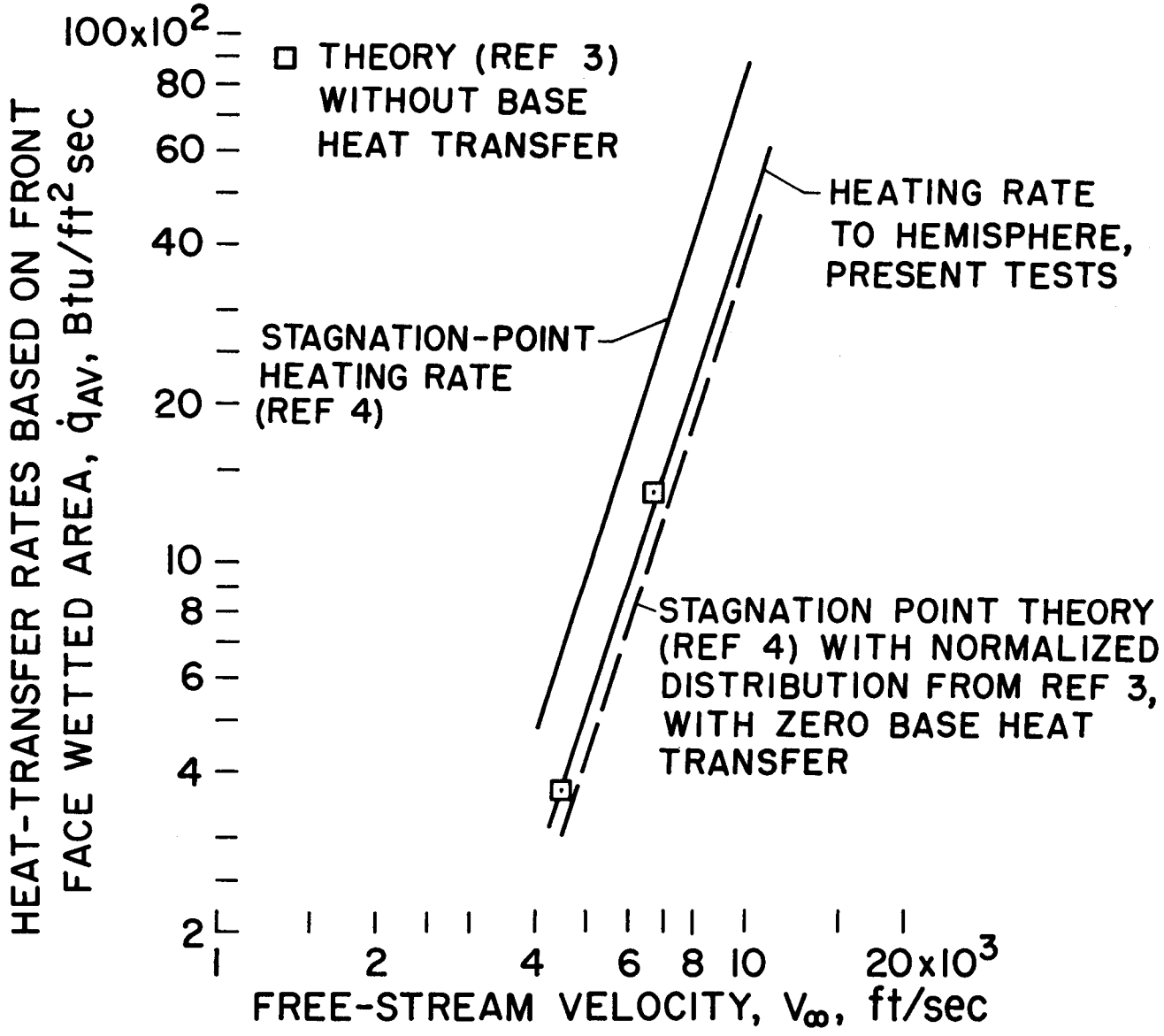

(b) Comparison of the experimental and theoretical heat-transfer rates, based on front face wetted area, for a 0.25-inch-diameter hemisphere.

Figure 6.- Concluded.

NATIONAL AERONAUTICS AND SPACE ADMINISTRATION
AMES RESEARCH CENTER, MOFFETT FIELD, CALIFORNIA

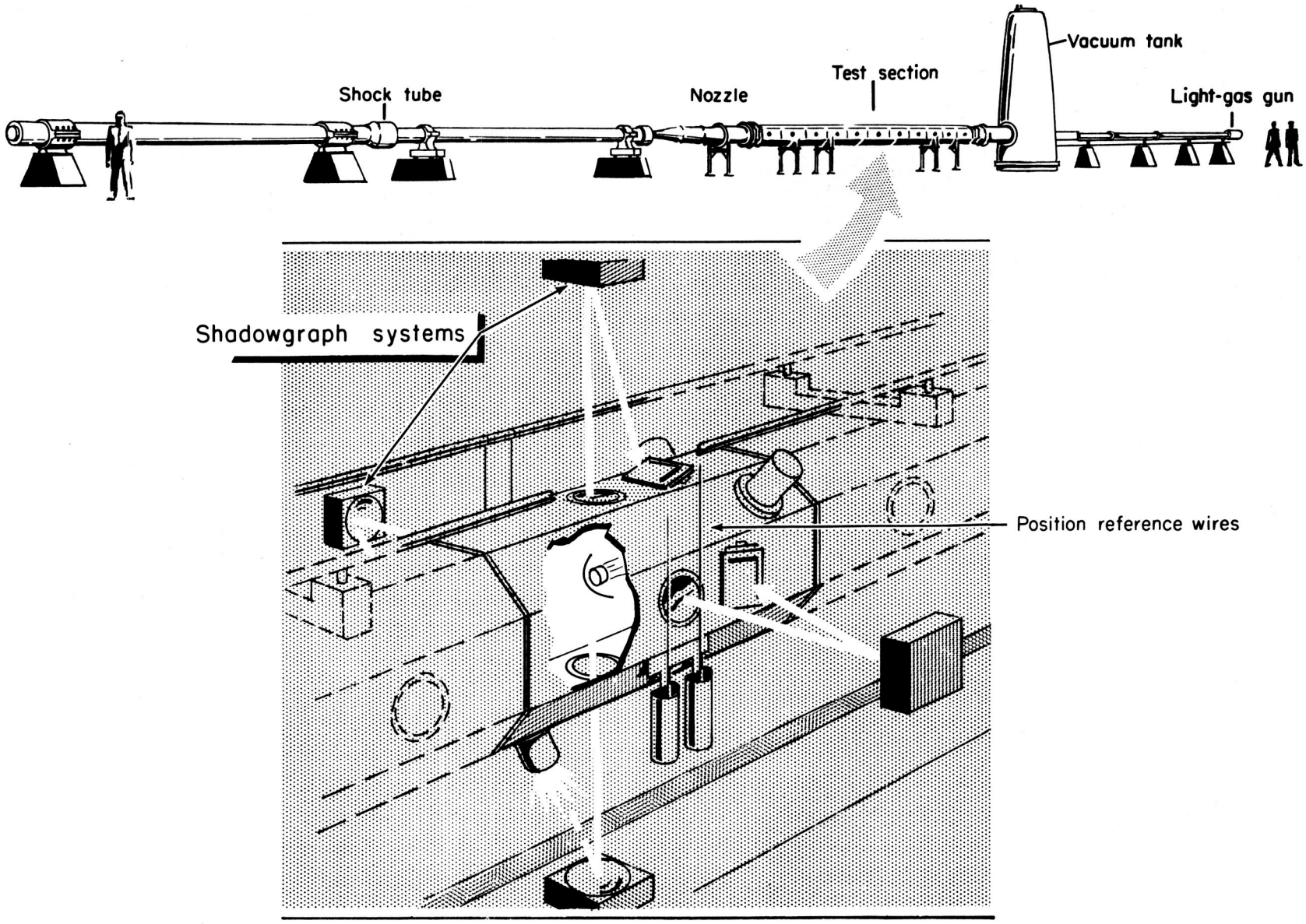

Figure 7.- Schematic drawing of prototype hypersonic free-flight facility.

NATIONAL AERONAUTICS AND SPACE ADMINISTRATION
AMES RESEARCH CENTER, MOFFETT FIELD, CALIFORNIA

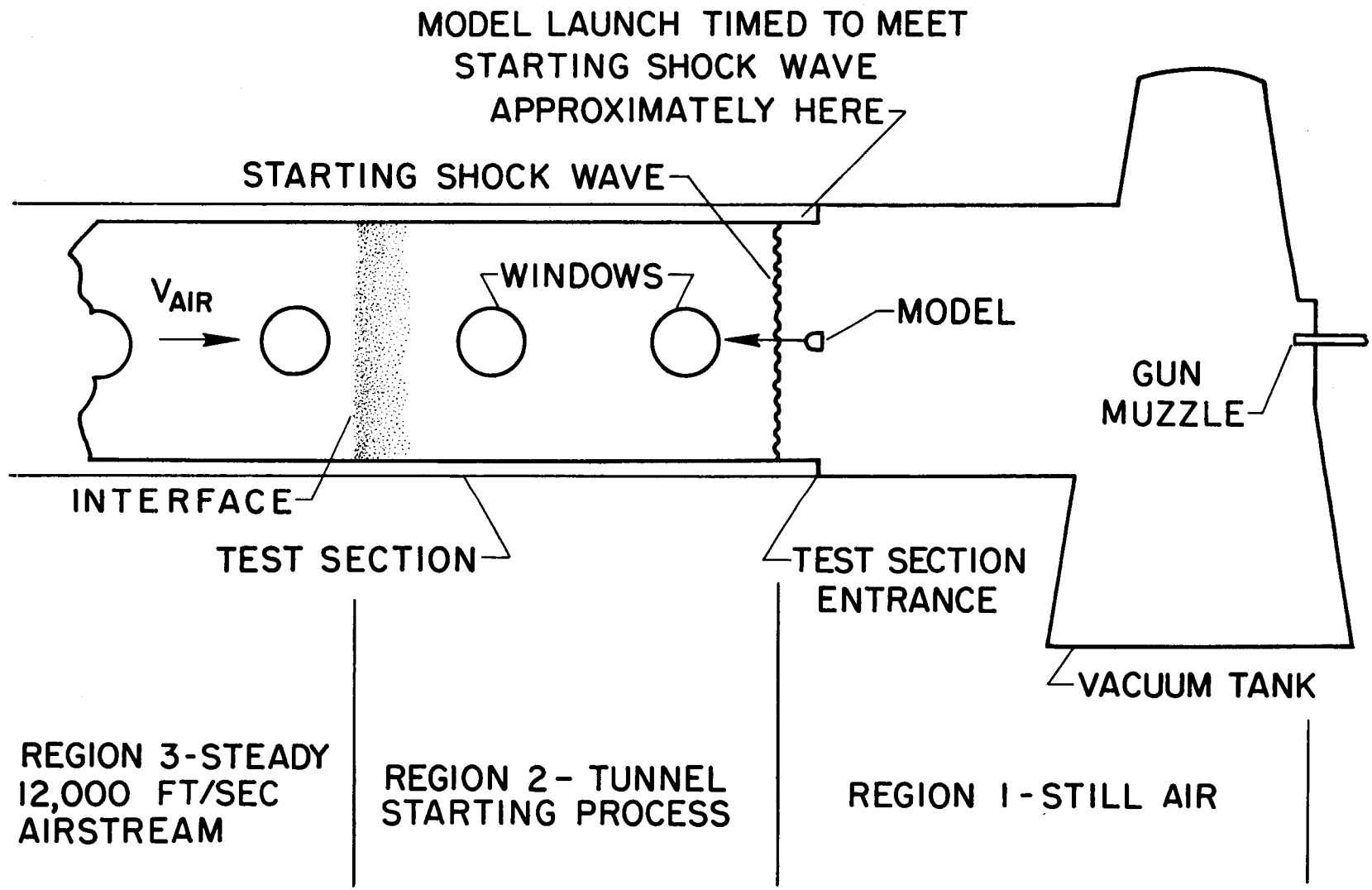

Figure 8.- Schematic for air-on operation. Not to scale.

NATIONAL AERONAUTICS AND SPACE ADMINISTRATION
AMES RESEARCH CENTER, MOFFETT FIELD, CALIFORNIA

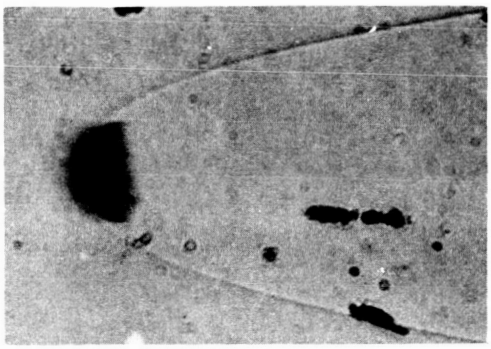

STA. 1; t = 0.634 ms;
T_w = 1020° F

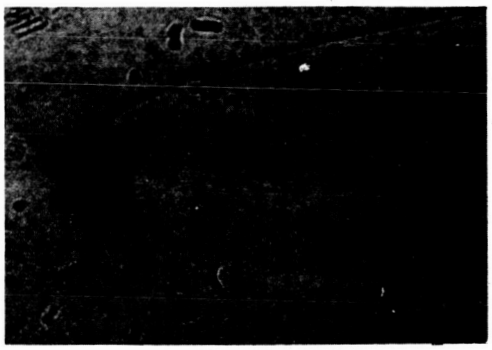

STA. 2; t = 0.807 ms;
T_w = 1116° F

STA. 3; t = 0.983 ms;
T_w = 1198° F
(MELTING FIRST OBSERVED)

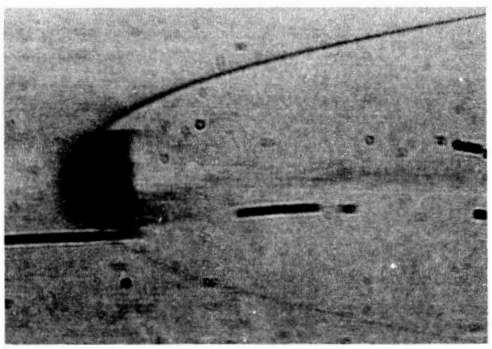

STA. 4; t = 1.161 ms;
T_w = 1267° F

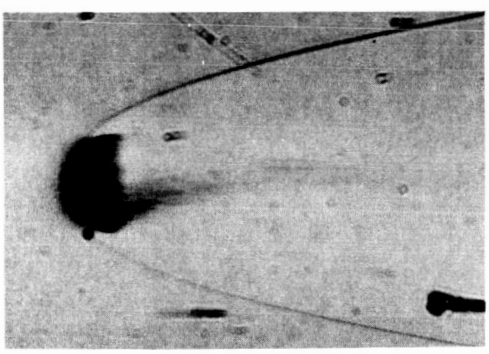

STA. 5; t = 1.341 ms;
T_w = 1327° F

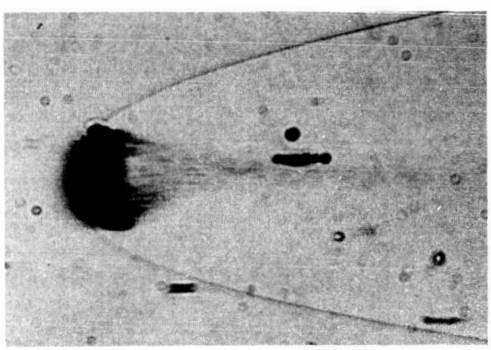

STA. 6; t = 1.523 ms
T_w = 1378° F

ALUMINUM (7075-T 6) MELTING TEMP. = 1180° F
V_L = 24,200 FT/SEC

Figure 9.- Shadowgraphs showing onset of melting.

NATIONAL AERONAUTICS AND SPACE ADMINISTRATION
AMES RESEARCH CENTER, MOFFETT FIELD, CALIFORNIA

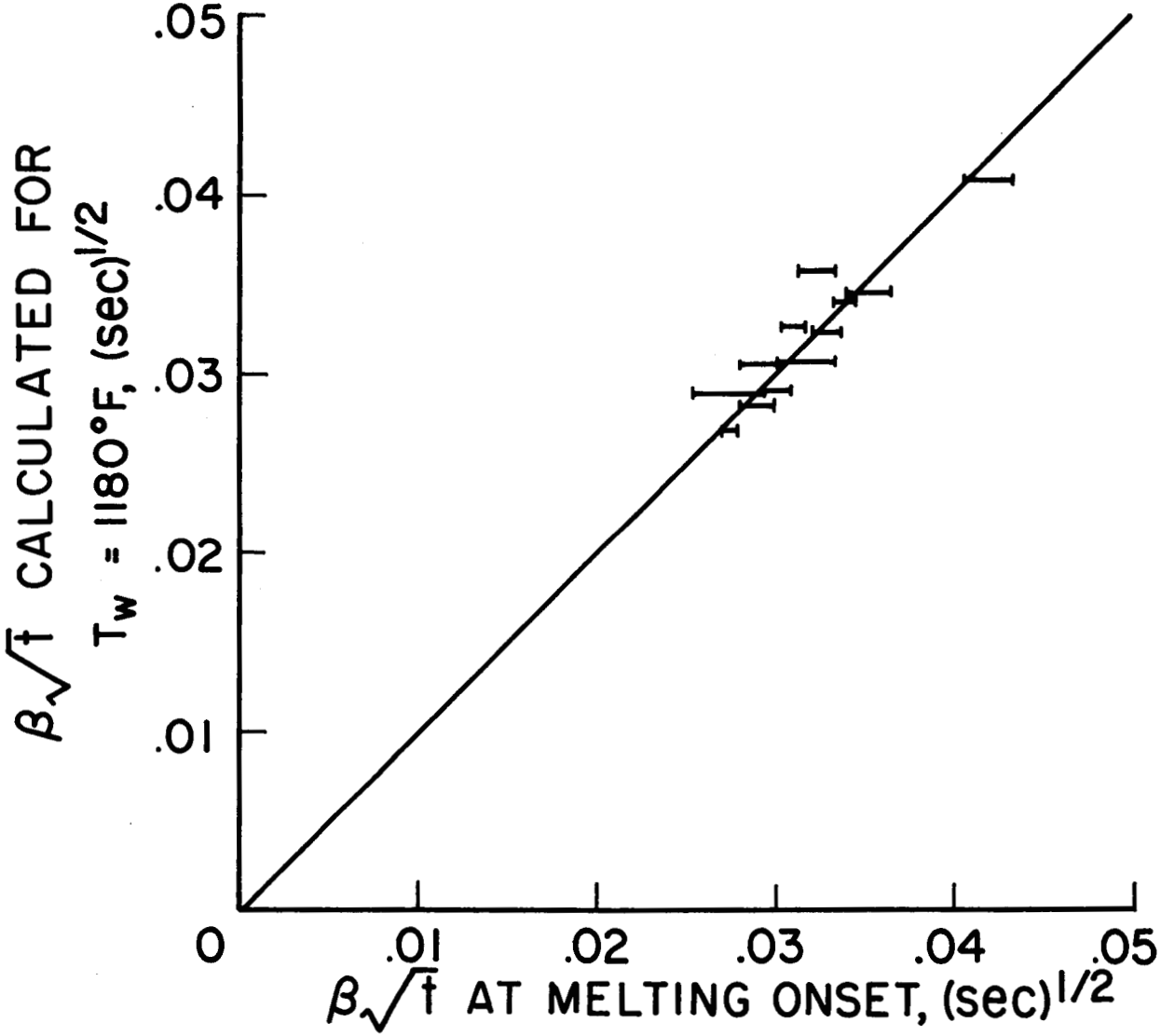

Figure 10.- Correlation plot for 24,000 ft/sec data.

NATIONAL AERONAUTICS AND SPACE ADMINISTRATION
AMES RESEARCH CENTER, MOFFETT FIELD, CALIFORNIA

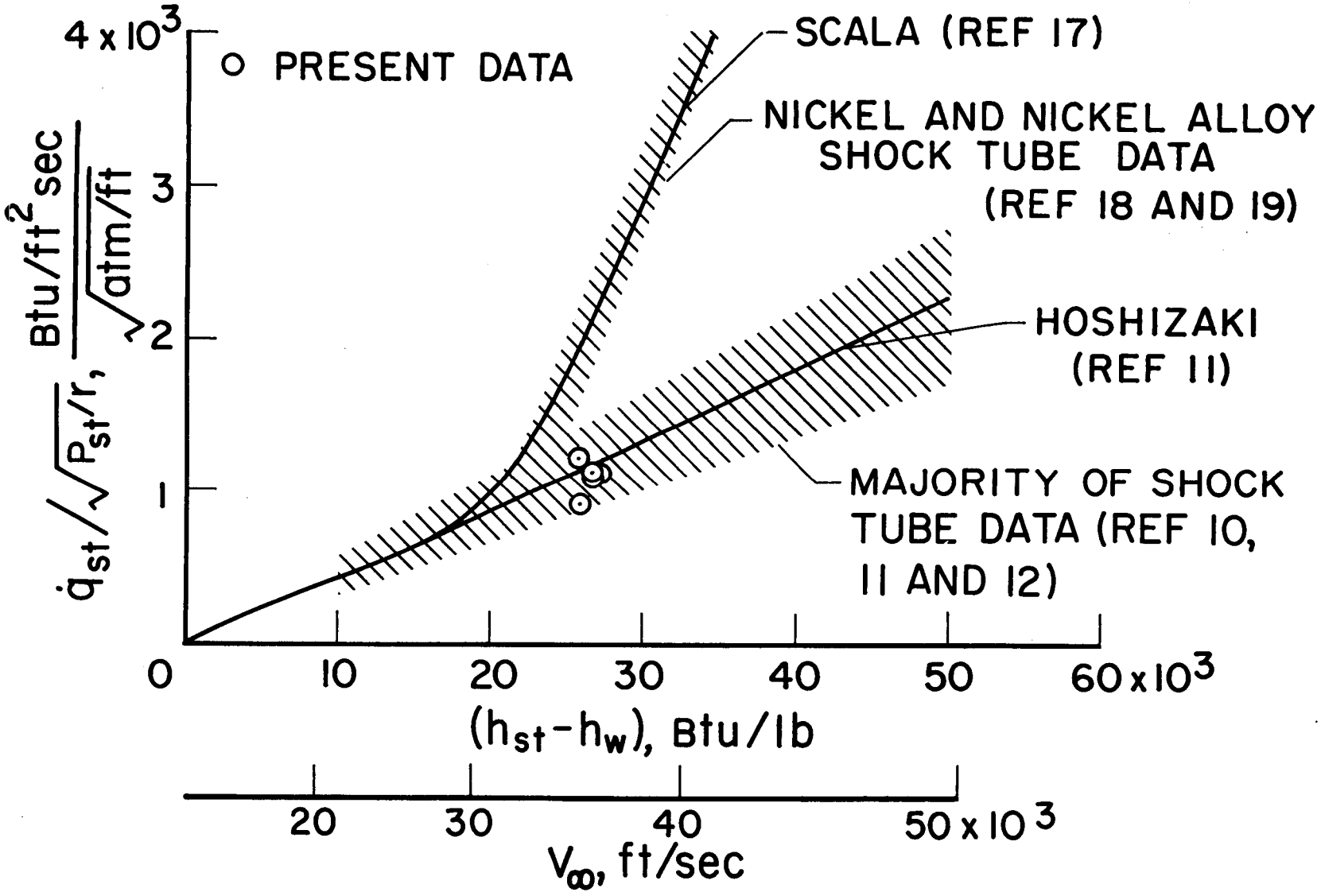

Figure 11.- Data taken at 36,000 ft/sec.

NATIONAL AERONAUTICS AND SPACE ADMINISTRATION
AMES RESEARCH CENTER, MOFFETT FIELD, CALIFORNIA